J. Synchrotron Rad. (1996). **3**, 282–288

Design of a Holographically Recorded Plane Grating with a Varied Line Spacing for a Soft X-ray Grazing-Incidence Monochromator

Kenta Amemiya,[a] Yoshinori Kitajima,[b] Toshiaki Ohta[a] and Kenji Ito[b]

[a]Department of Chemistry, Graduate School of Science, The University of Tokyo, Hongo, Tokyo 113, Japan, and [b]Photon Factory, National Laboratory for High Energy Physics, Oho, Tsukuba, Ibaraki 305, Japan. E-mail: kenji.ito@kek.jp

(*Received 22 April 1996; accepted 24 June 1996*)

A new design concept is presented for a plane grating with a varied line spacing for the Monk–Gillieson mounting monochromator. A light path function including both a spherical mirror and a varied-line-spacing grating is defined to optimize groove parameters. Aspheric wavefront recording optics are utilized to fabricate a grating holographically. Ray-tracing results show that the varied-line-spacing grating eliminates aberrations significantly and affords a high resolving power as a total optical system of a soft X-ray grazing-incidence monochromator. The effects of errors in recording parameters and in the radius of the spherical mirror are described, and possible ways to compensate for these errors are discussed.

Keywords: varied line spacing; holographic grating; grazing-incidence monochromators; soft X-rays; aspheric wavefront recording.

1. Introduction

Over the past decade, many types of grazing-incidence monochromators for soft X-rays have been developed at various synchrotron radiation facilities (Petersen, Jung, Hellwig, Peatman & Gudat, 1995; Chen, 1987; Ishiguro *et al.*, 1989; Padmore, 1989). Among them, Hettrick, Underwood, Batson & Eckart (1988) proposed a monochromator system of the Monk–Gillieson mounting (Monk, 1928; Gillieson, 1949) combined with a varied-line-spacing (VLS) plane grating. This type of grazing-incidence monochromator is capable of providing a stable monochromatic beam and high resolving power because scanning the photon energy does not require any linear translation of all the optical elements but only the rotation of the grating. Although the scanning mechanism itself is quite simple, it is essential to use a high-quality VLS grating to achieve high performance. Efforts should be made to optimize the groove parameters in order to correct aberrations, and to realize these improvements in the manufacturing process.

For optimization of the groove parameters for the Hettrick-type monochromator in previous studies (Callcott *et al.*, 1992; McKinney, 1992), a light path function was defined for the grating alone assuming that the grating is illuminated by perfectly converging rays in the plane of dispersion. Recently, Koike, Beguiristain, Underwood & Namioka (1994) pointed out that the use of such a light path function is not appropriate because it cannot take the coma and higher-order aberrations of the focusing elements into account correctly. Instead, they have utilized ray-traced spot diagrams and a merit function to obtain the optimum spacing variation. However, it is more useful to develop a light path function including a focusing element explicitly to obtain the optimized groove parameters and estimate the tolerances.

There are two major techniques used for the production of gratings for soft X-rays, *i.e.* mechanical ruling and holographic recording. Laminar-shaped holographic gratings, because of their smooth surfaces, have been used increasingly for several years for the efficient suppression of higher spectral orders and scattered light. However, the standard holographic technique is not capable of producing VLS gratings because it apparently fails to eliminate aberrations sufficiently. One solution to this problem is to use an aspheric wavefront recording optics. Noda, Harada & Koike (1989) showed an aspheric wavefront to result from the installation of spherical mirrors between the laser source and the grating blank. They produced a holographic grating for a Seya–Namioka monochromator with this method and achieved a greatly improved resolution compared with gratings recorded by a spherical wavefront. Analytical formulae for this type of grating were advanced by Namioka & Koike (1995) and recording techniques have been proposed by the Shimadzu Corporation (Harada, Koike & Noda, 1989). Recently, Koike (1995) demonstrated the possibility of using an aspheric holographic VLS grating for a grazing-incidence monochromator.

The purpose of this paper is to design, in a more comprehensive way, a holographically recorded plane grating with a varied line spacing for a soft X-ray grazing-incidence

monochromator. In §2 we derive a light path function involving both a focusing spherical mirror and a grating. In §3 we show how to optimize the groove parameters of VLS gratings for a new soft X-ray grazing incidence monochromator that will be constructed at beamline 11A of the Photon Factory. In §4 we examine the validity of the aspheric wavefront holographic recording method for the case of the soft X-ray grazing-incidence monochromator. In §5 we estimate the degradation of the resolving power that may arise from errors in manufacturing of the grating and from variations in the radius of the spherical mirror.

2. Derivation of the light path function

The optical system of a Hettrick-type monochromator (Hettrick *et al.*, 1988) is shown schematically in Fig. 1. The origin, O, of the Cartesian coordinate system is at the centre of the grating, G, the x axis is the normal to the grating surface at O, and the y and z axes are perpendicular and parallel to the grooves, respectively. The point source, A (corresponding to the centre of the entrance slit), a spherical mirror, M_A, and G are arranged so that A, O_A (vertex of M_A), the normal of M_A, and O lie in the xy plane. Consequently, the principal rays originating at A pass through O_A, O and a focusing point B (the centre of the exit slit). The distances between the optical elements are defined as $p_A = AO_A$, $q_A = O_AO$, and $r_B = OB$. An additional Cartesian coordinate system $x_Ay_Az_A$ is defined with M_A; its origin is O_A, the x_A axis is the mirror normal at O_A, and the y_A axis lies in the xy plane. The angles α, β and η_A are defined as shown in Fig. 1.

Assuming that the light passes through B after having been reflected at P_A (ξ_A, w_A, l_A) and diffracted at P (ξ, w, l) on the nth groove from the centre of the grating, the light path function, F, is given by

$$F = AP_A + P_AP + PB + nm\lambda, \tag{1}$$

where m is the diffraction order (+1 throughout this paper) and λ is the wavelength of light. We can expand the first three terms in (1) into a power series in w and l as follows:

$$\begin{aligned} F = {} & p_A + q_A + r_B + M_{10}w \\ & + (M_{20}w^2 + M_{02}l^2 + M_{30}w^3 + M_{12}wl^2)/2 \\ & + (M_{40}w^4 + 2M_{22}w^2l^2 + M_{04}l^4)/8 + \ldots + nm\lambda. \end{aligned} \tag{2}$$

The coefficients M_{ij} are obtained in a similar way to Namioka & Koike (1995):

$$\begin{aligned} M_{10} &= -\sin\alpha - \sin\beta, \\ M_{20} &= \cos^2\alpha/r_A + \cos^2\beta/r_B, \\ M_{30} &= \sin\alpha\cos^2\alpha/r_A^2 + \sin\beta\cos^2\beta/r_B^2 \\ &\quad - 2(A_{10})_A^2K_A\sin\eta_A/R_A, \\ M_{40} &= \cos^2\alpha(4\sin^2\alpha/r_A - \cos^2\alpha/r_A)/r_A^2 \\ &\quad + \cos^2\beta(4\sin^2\beta/r_B - \cos^2\beta/r_B)/r_B^2 \\ &\quad + 2(A_{10})_A^2K_A(E_{40})_A\cos\eta_A/R_A \\ &\quad + 2(A_{10})_A^3[\cos\alpha/r_A\cos\eta_A \\ &\quad - (A_{10})_A\cos\eta_A/R_A]/R_A^2, \\ &\ldots \end{aligned} \tag{3}$$

where

$$\begin{aligned} r_A &= q_A + (1/p_A - 2\sec\eta_A/R_A)^{-1}, \\ (A_{10})_A &= -\cos\alpha/A_Aq_A\cos\eta_A, \\ A_A &= 1/p_A + 1/q_A - 2\sec\eta_A/R_A, \\ K_A &= \cos\alpha/r_A - (A_{10})_A/R_A, \\ (E_{40})_A &= -\cos\alpha[1 + \tan\eta_A(7\tan\eta_A + 12\tan\alpha)]/r_A \\ &\quad + 3K_A\tan^2\eta_A[1 + 6(A_{10})_Aq_A/R_A\cos\alpha]. \end{aligned} \tag{4}$$

The third term in M_{30} and the third and fourth terms in M_{40} are new and arise from taking the spherical mirror into consideration. The groove number, n, is also expanded into a power series in w and l,

$$\begin{aligned} n = {} & (1/\lambda_0)[n_{10}w + (n_{20}w^2 + n_{02}l^2 + n_{30}w^3 + n_{12}wl^2)/2 \\ & + (n_{40}w^4 + 2n_{22}w^2l^2 + n_{04}l^4)/8 + \ldots], \end{aligned} \tag{5}$$

where λ_0 is the wavelength of light being used for the holographic recording. The light path function is rewritten:

$$F = p_A + q_A + r_B + \sum_{ij} a_{ij}(M_{ij} + mn_{ij}\lambda/\lambda_0) \tag{6}$$

where $(i + j \geq 1, j$ even) and coefficients a_{ij} $(i + j \leq 4)$ are

$$\begin{aligned} a_{10} &= 1, \quad a_{20} = a_{02} = a_{30} = a_{12} = 1/2 \\ a_{22} &= 1/4, \quad a_{40} = a_{04} = 1/8. \end{aligned} \tag{7}$$

If

$$F_{ij} = M_{ij} + mn_{ij}\lambda/\lambda_0 = 0 \tag{8}$$

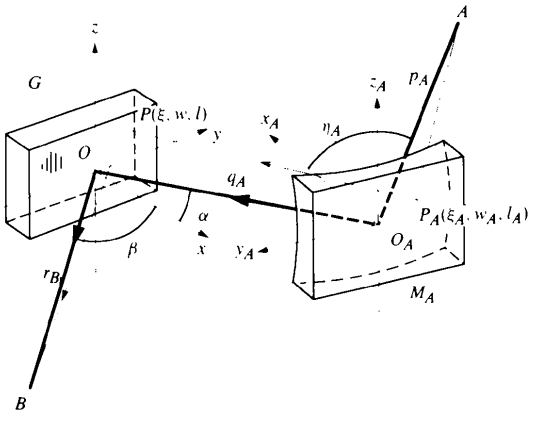

Figure 1
Schematic diagram of the Hettrick-type VLS grating monochromator.

for all (i, j) at any λ, a perfect focus is obtained. It requires all M_{ij}/λ to be constant over the whole scanned-wavelength range, which is impossible in the present optical system.

3. Optimization of groove parameters

In this section we will describe the optimization procedure of a VLS grating for the new monochromator that will be installed at beamline 11A of the Photon Factory. The groove parameters for the VLS grating will be obtained using the light path function derived in the previous section. Fig. 2 shows the optical layout for the new beamline which is designed to cover the energy range 200–1300 eV. The length of the monochromator, from the entrance slit, $S1$, to the exit slit, $S2$, is ~ 6 m. Horizontal focusing is carried out by a Pt-coated cylindrical mirror, $M0$, and a second cylindrical mirror, $M0'$, achieves vertical focusing. Either spherical mirror, M_1 or M_2, playing the role of M_A in the previous section, is interchangeably used, depending on the desired photon energy range, to focus rays in the plane of dispersion on an imaginary point 3 m behind the grating. Deviation angles at the grating, G, are 176.2 and 173.8°, corresponding to M_1 and M_2, respectively. Monochromatic light from $S2$ is refocused on the sample position by a toroidal mirror, M_f. The incidence angles, radii of curvature and dimensions for the optical elements used in this beamline are summarized in Table 1.

Here we consider an 800 lines mm^{-1} grating, which corresponds to $n_{10} = 0.35328$ for $\lambda_0 = 4416.0$ Å. In the previous methods (Hettrick *et al.*, 1988; McKinney, 1992), $F_{20} = 0$ is satisfied at two energies using two parameters (r_A/r_B and n_{20} in our notation). However, we keep r_A/r_B fixed at -1 and determine $n_{20} = -0.23514$ m^{-1} in order to satisfy the condition $F_{20} = 0$ for the spherical mirror M_2 at just one energy of 500 eV. In other words, $F_{20} = 0$ is realized for zeroth order light ($m = 0$ and $\alpha = -\beta$) and at 500 eV. The reason we adopt $r_A/r_B = -1$ will become clearer in §5 where we discuss the need for compensation of errors in the mirror

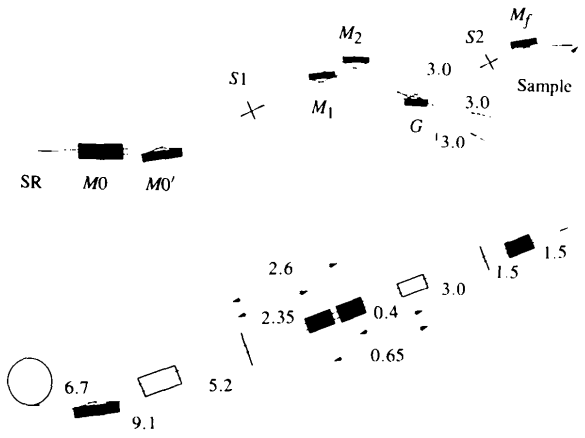

Figure 2
Schematic side view (top) and top view (bottom) of a new grazing-incidence monochromator. Distances between optical elements are indicated in m.

Table 1
Optical parameters of mirrors in the monochromator for Photon Factory beamline 11A.

	Incidence angle (°)	Shape	Radius (m)	Dimensions (mm)
$M0$	88.0	Cylindrical	370.0	1000 × 60
$M0'$	88.0	Cylindrical	224.6	600 × 60
M_1	88.1	Spherical	86.19	200 × 50
M_2	86.9	Spherical	54.49	200 × 50
G		Plane		140 × 50
M_f	88.0	Toroidal	43.0 (m), 0.104 (s)	250 × 50

radius R_A. In spite of these boundary conditions, M_{20}/λ and the focal length remain rather constant, as shown in Fig. 3. We also set $n_{30} = 0.0714$ m^{-2} and $n_{40} = -0.0983$ m^{-3} so that $F_{30} = 0$ and $F_{40} = 0$ at 500 eV. If they were optimized using the light path function for the grating alone, $n_{30} = 0.0781$ m^{-2} and $n_{40} = -0.104$ m^{-3} would be obtained while n_{20} would be the same as in the present optimization.

In order to check the validity of the new light path function, we have estimated the resolving power by the method of ray tracing. The ray-tracing program *SRXRAY* (Muramatsu, Ohishi & Maezawa, 1988) was used with some modifications. The source size and divergence of the synchrotron radiation were estimated at $\sigma_x = 1.263$, $\sigma_y = 0.206$ mm, $\sigma_x' = 0.394$ and $\sigma_y' = 0.037$ mrad using the parameters for bending magnet No. 11 of the Photon Factory (Katoh & Hori, 1993). About 40 000 rays are generated in the horizontal divergence of 4 mrad without any vertical restriction at the source point. To evaluate the

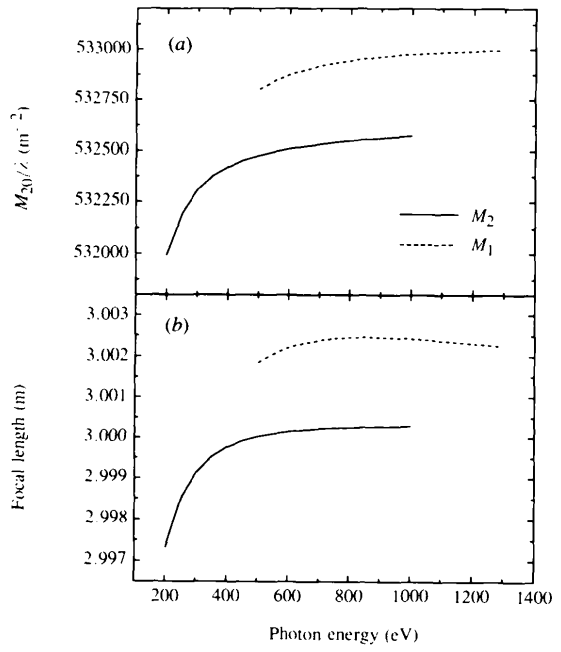

Figure 3
(*a*) Variation of M_{20}/λ as a function of photon energy, and (*b*) focal length as a function of photon energy obtained by solving $F_{20} = 0$ about r_B when M_2 (solid line) and M_1 (dashed line) are used.

resolving power, we adopt the method proposed by Koike & Namioka (1995). They defined the resolving power as $\mathcal{R} = \lambda/\Delta\lambda$, where $\Delta\lambda = 2.688 s_\lambda$, and s_λ is the product of the standard deviation of ray-traced spots in the direction of dispersion and the reciprocal linear dispersion at λ. The entrance slit width is chosen to be 10 μm to emphasize the effects of aberrations.

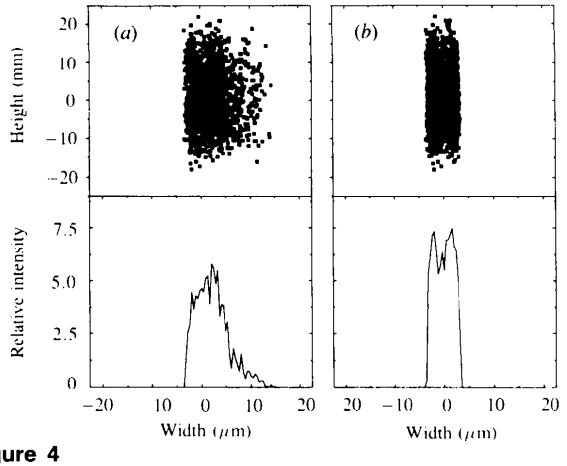

Figure 4
Spot diagrams and line profiles of ray-traced spots at the exit slit for two different optimization methods: (*a*) using the light path function for the grating alone, and (*b*) using the light path function including the spherical mirror M_2.

Fig. 4 shows spot diagrams and line profiles at the exit slit in two cases: (*a*) n_{20}, n_{30} and n_{40} have been optimized using the light path function for the grating alone; (*b*) the optimization includes the spherical mirror. In both cases all other n_{ij} are fixed to zero, which corresponds to straight grooves. The difference between the two methods is obvious. We have also calculated the resolving power as a function of n_{20}, n_{30} and n_{40}. In these calculations one of n_{20}, n_{30} and n_{40} was varied while the other two parameters were kept fixed at the optimized values. As shown in Fig. 5, the resolving power reaches a maximum at around the optimized values of n_{i0} indicated by arrows. The results of optimization using the new light path function are thus verified with the help of the ray-tracing method.

Since we use either M_1 or M_2 as a spherical mirror, we should optimize the groove parameters so that sufficient resolution can be attained for both mirrors. To meet this demand, we also optimize n_{20}, n_{30} and n_{40} for M_1 at 1000 eV, and simply take averages of the optimized values for M_1 and M_2. They are $n_{20} = -0.23525\ \mathrm{m}^{-1}$, $n_{30} = 0.0718\ \mathrm{m}^{-2}$ and $n_{40} = -0.0951\ \mathrm{m}^{-3}$. Fig. 6 shows the resolving power when these values are adopted but other n_{ij} are set to zero. We can obtain a resolving power of more than 5000 for 200–1300 eV if the mirror is chosen properly. The present parameters are directly applicable to mechanically ruled gratings with straight grooves.

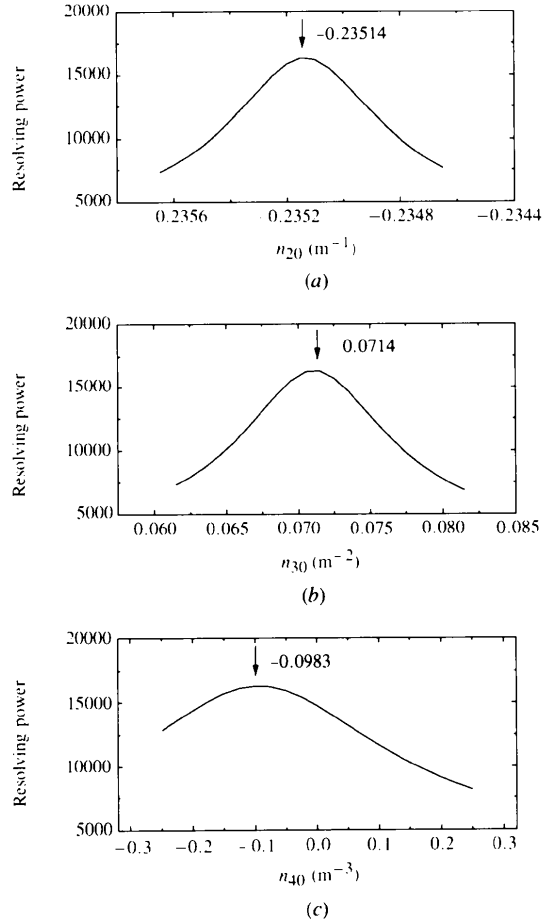

Figure 5
Resolving power as a function of groove parameter n_{20} (*a*), n_{30} (*b*) and n_{40} (*c*). As one parameter is changed, other parameters are kept at the optimized values.

4. Recording parameters for the holographic grating

The optical system for an aspheric wavefront recording is shown in Fig. 7. This is essentially the same as Fig. 1, with C, D, γ and δ having been substituted for A, B, α and β, respectively. However, D is not an imaging point but a light source, as is C. The groove parameters n_{ij} ($i + j \leq 4$) can be expressed as a function of R_C, p_C, q_C, r_D, γ, δ and η_C, based on the derivations by Namioka & Koike (1995). Although they considered two inserted ellipsoidal

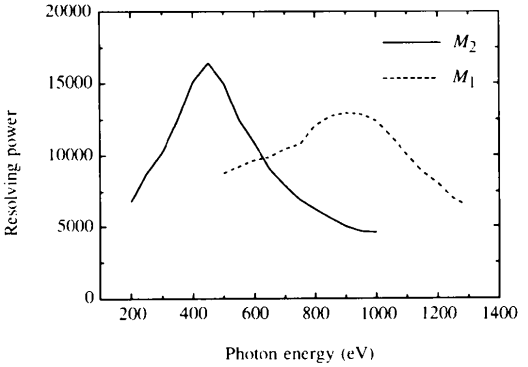

Figure 6
Evaluated resolving powers for the straight-groove VLS grating when M_2 (solid line) or M_1 (dashed line) is used.

mirrors and an ellipsoidal grating, their general equations are easily applied to our system consisting of one spherical mirror and a plane grating:

$$
\begin{aligned}
n_{10} &= \sin\delta - \sin\gamma,\\
n_{20} &= \cos^2\gamma/r_C - \cos^2\delta/r_D,\\
n_{30} &= \sin\gamma\cos^2\gamma/r_C^2 - \sin\delta\cos^2\delta/r_D^2\\
&\quad - 2(A_{10})_C^2 K_C \sin\eta_C/R_C,\\
n_{40} &= \cos^2\gamma(4\sin^2\gamma/r_C - \cos^2\gamma/r_C)/r_C^2\\
&\quad - \cos^2\delta(4\sin^2\delta/r_D - \cos^2\delta/r_D)/r_D^2\\
&\quad + 2(A_{10})_C^2 K_C (E_{40})_C \cos\eta_C/R_C\\
&\quad + 2(A_{10})_C^3[\cos\gamma/r_C\cos\eta_C\\
&\quad - (A_{10})_C\cos\eta_C/R_C]/R_C^2,\\
&\cdots
\end{aligned}
\tag{9}
$$

where r_C, $(A_{10})_C$, K_C and $(E_{40})_C$ are defined by (4), substituting C and γ for A and α, respectively.

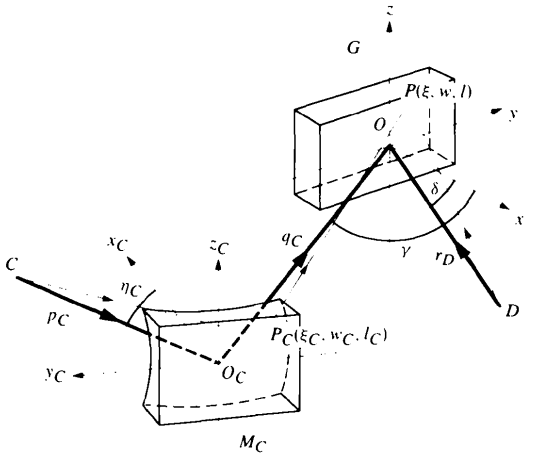

Figure 7
Schematic diagram of an aspheric wavefront holographic recording system.

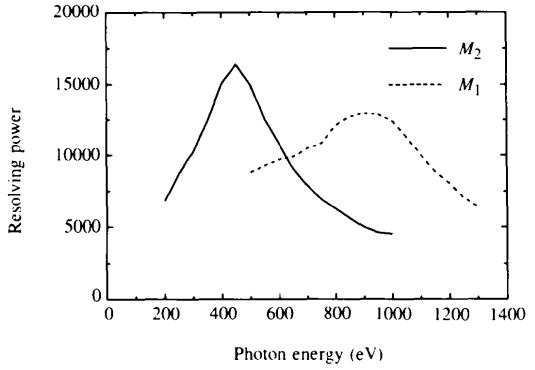

Figure 8
Evaluated resolving powers for the holographic VLS grating when M_2 (solid line) or M_1 (dashed line) is used.

Table 2
Groove parameters n_{ij} for the holographic VLS grating.

n_{10}	0.35328	n_{12}	0.03870 m^{-2}
n_{20}	−0.23525 m^{-1}	n_{40}	−0.09509 m^{-3}
n_{02}	0.06365 m^{-1}	n_{22}	0.02328 m^{-3}
n_{30}	0.07180 m^{-2}	n_{04}	0.04122 m^{-3}

For simplicity, we solved only the four equations for n_{10}, n_{20}, n_{30} and n_{40}, choosing γ, δ, r_D and η_C as the optimization parameters. The other recording parameters can be chosen arbitrarily so that they are of practical size without making n_{ij} other than n_{10}, n_{20}, n_{30} and n_{40} too large. The recording parameters determined here are p_C = 1.35, q_C = 0.55, r_D = 2.5090 m, γ = 42.756, δ = −19.002, η_C = 34.360°, R_C = 5.0 m. The groove parameters n_{ij} obtained from these recording parameters are listed in Table 2.

Fig. 8 shows the resolving power of this holographic VLS grating evaluated by the ray-tracing method; the result is almost the same as in Fig. 6 for straight grooves. This means that n_{ij} other than n_{10}, n_{20}, n_{30} and n_{40} have little effect on resolution, at least as long as they remain rather small. Thus, it is feasible to produce a holographic VLS grating with a laminar shape, which is effective in suppression of higher order and scattered light, without any significant loss in resolving power.

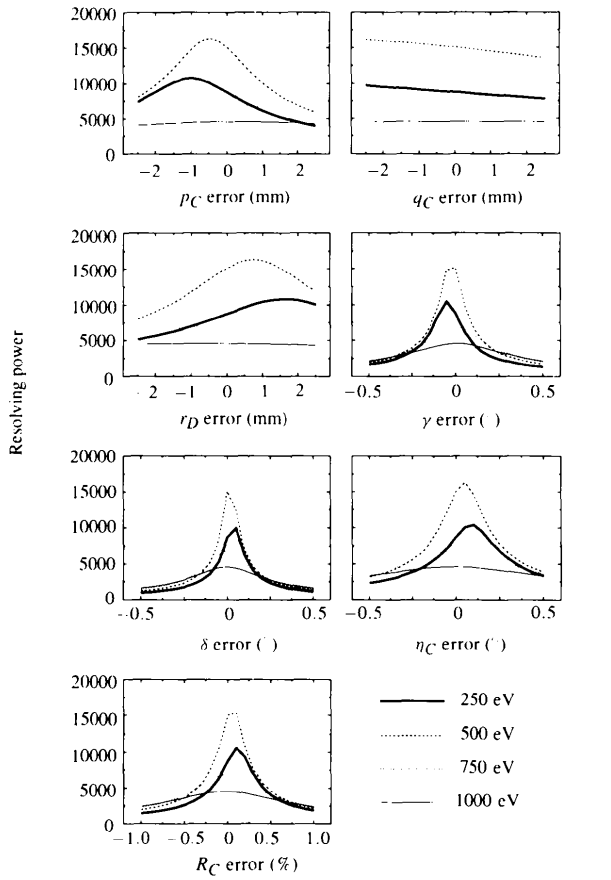

Figure 9
Effects of errors in the recording parameters on the resolving power at four typical energies when M_2 is used.

5. Effects of, and compensation for, manufacturing errors of the optical components

From a practical point of view it is important to estimate the effects of deviations from the designed values in manufacturing optical components. Fig. 9 shows the degradation in the resolving power as a function of deviations in the recording parameters of the grating at four typical energies (shown only for M_2). As shown in Figs. 10(a) and 10(b) for δ, the decrease in resolving power is largely due to changes in n_{20} which lead to corresponding shifts in the focal length. Theoretically, we can compensate for these errors by tracking the focal point by an analogous translation of the exit slit (see Fig. 10c). However, in accordance with our initial concept of a monochromator with stable beam characteristics, it is not desirable to move the exit slit during the energy scan. If we want a resolving power of more than 4000 without moving the exit slit during a wide energy scan, the shift in the focal length for 250–1000 eV must be less than 10 mm, requiring the error of δ to be within $\pm 0.2°$. Of course, errors will occur in other parameters and can make things worse.

Fortunately, the error in R_C (radius of M_C) can be compensated for if its real value is precisely known. Indeed, R_C can be measured with a precision of 0.01%. Since R_C is not an optimization parameter, we only have to solve the above-mentioned equations in order to find the best values of n_{10}, n_{20}, n_{30} and n_{40}.

Another possible error may exist in the radius of the spherical mirror of the monochromator. Fig. 11(a) shows the effects on the resolving power of errors in R_2 (radius of spherical mirror M_2). The resolving power is found to change rapidly with r_A as shown in Fig. 11(b). In order to compensate for this error, we set $r_A = -r_B$ by changing η_A, p_A and q_A accordingly, keeping the principal ray to illuminate the centres of the spherical mirror and of the grating. Practically, rotations of *ca* 0.1 and 0.06° and translations of 10 and 20 mm for M_2 and M_1, respectively, are necessary in order to compensate for possible errors of 3% in their radii. For these adjustments we have to provide a mechanism for changing the incidence angles of M_1 and M_2 as well as their positions along the direction of the incident rays. The reason we adopt $r_A = -r_B$ is as follows: we know that these mirrors are located properly, *i.e.* that

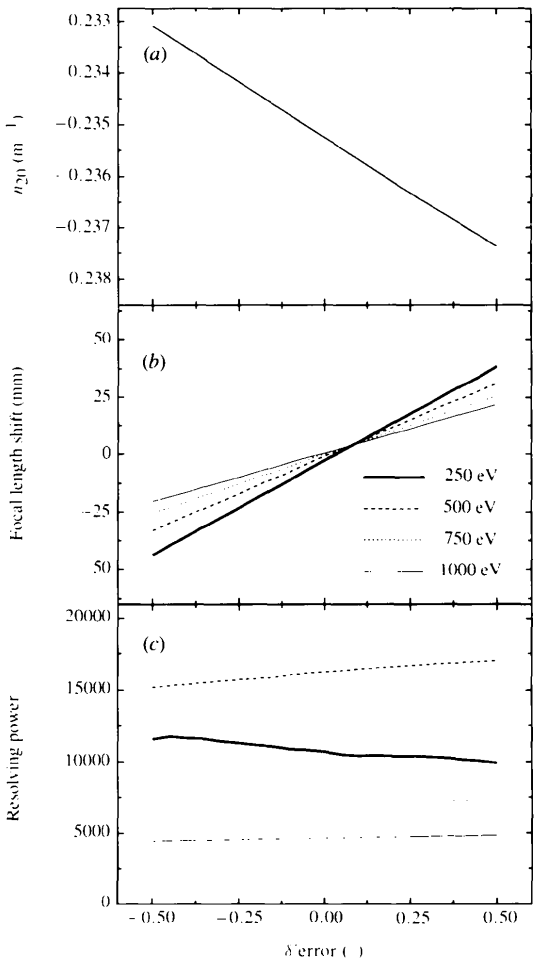

Figure 10
Effects of errors in δ and their compensation: (a) variation of the groove parameter n_{20}, (b) change of focal length, and (c) resolving power when the exit slit is translated by the value shown in (b).

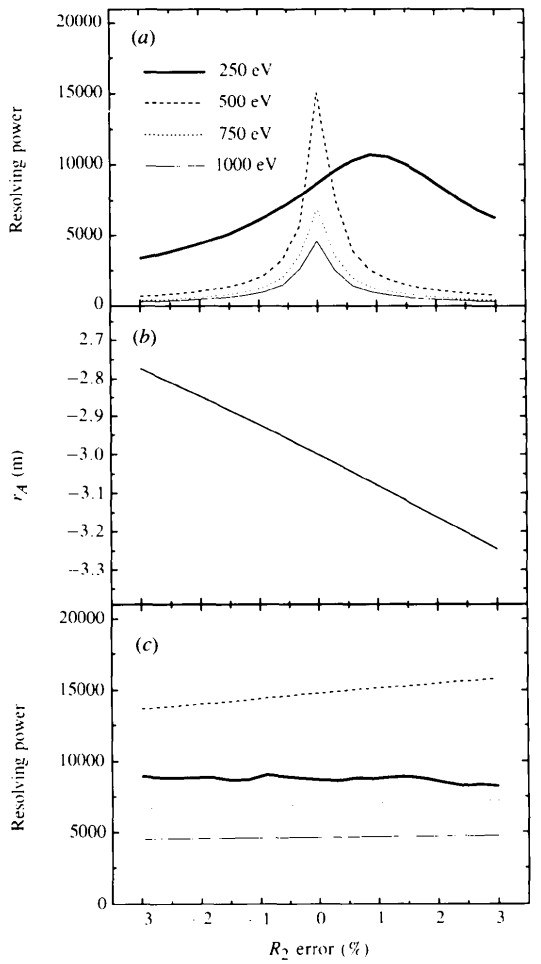

Figure 11
Effects of errors in R_2 (radius of M_2) and their compensation: (a) decrease in the resolving power, (b) variation of r_A, (c) resolving power after proper compensation.

$r_A = -r_B$ is satisfied when the zeroth-order rays are found to be focused on the exit slit. It should be noted that this compensation is independent of photon energy and that no adjustment is necessary during the energy scan. When this compensation is carried out, the resolving power is almost perfectly restored, as shown in Fig. 11(*c*).

6. Conclusions

We have proposed a new design concept for a VLS plane grating for the Monk–Gillieson mounting monochromator. It has been shown that the groove parameters can be optimized directly using a light path function including both a spherical mirror and a grating.

It has also been demonstrated that aspheric wavefront recording optics are available for producing a holographic VLS grating that has a resolving power that is as high as that of a mechanically ruled grating. We can expect to suppress higher spectral orders and scattered light efficiently by using a laminar-shaped grating at the new beamline (PF-BL-11A) that is under construction.

Finally, we have evaluated the effects of errors in manufacturing optical components on the resolving power. The tolerances for the deviations of recording parameters were estimated and a method of compensating for the errors in the radii of the spherical mirrors of the monochromator was proposed. We believe that such information is essential if high-resolution monochromators for synchrotron radiation are to achieve their desired performance.

We would like to thank Drs Masato Koike (Lawrence Berkeley Laboratory), Eiji Ishiguro (Ryukyu University), Kazuo Sano (Shimadzu Corporation) and Klaus P. Huber (NRC, Canada) for valuable discussions.

References

Callcott, T. A., O'Brien, W. L., Jia, J. J., Dong, Q. Y., Ederer, D. L., Watts, R. N. & Mueller, D. R. (1992). *Nucl. Instrum. Methods*, A**319**, 128–134.
Chen, C. T. (1987). *Nucl. Instrum. Methods*, A**256**, 595–604.
Gillieson, A. H. C. P. (1949). *J. Sci. Instrum.* **26**, 335.
Harada, Y., Koike, M. & Noda, H. (1989). *Shimadzu Hyoron*, **44**, 365–375. (In Japanese.)
Hettrick, M. C., Underwood, J. H., Batson, P. J. & Eckart, M. J. (1988). *Appl. Opt.* **27**, 200–202.
Ishiguro, E., Suzui, M., Yamazaki, J., Nakamura, E., Sakai, K., Matsudo, O., Mizutani, N., Fukui, K. & Watanabe, M. (1989). *Rev. Sci. Instrum.* **60**, 2105–2108.
Katoh, M. & Hori, Y. (1993). KEK Report 92-20. National Laboratory for High Energy Physics, Tsukuba, Ibaraki 305, Japan. (In Japanese.)
Koike, M. (1995). *Hoshako*, **8**, 509–520. (In Japanese.)
Koike, M., Beguiristain, R., Underwood, J. H. & Namioka, T. (1994). *Nucl. Instrum. Methods*, A**347**, 273–277.
Koike, M. & Namioka, T. (1995). *Rev. Sci. Instrum.* **66**, 2144–2146.
McKinney, W. R. (1992). *Rev. Sci. Instrum.* **63**, 1410–1414.
Monk, G. S. (1928). *J. Opt. Soc. Am.* **17**, 358.
Muramatsu, Y., Ohishi, Y. & Maezawa, H. (1988). KEK Internal Report 87-10. National Laboratory for High Energy Physics, Tsukuba, Ibaraki 305, Japan. (In Japanese.)
Namioka, T. & Koike, M. (1995). *Appl. Opt.* **34**, 2180–2186.
Noda, H., Harada, Y. & Koike, M. (1989). *Appl. Opt.* **28**, 4375–4380.
Padmore, H. A. (1989). *Rev. Sci. Instrum.* **60**, 1608–1615.
Petersen, H., Jung, C., Hellwig, C., Peatman, W. B. & Gudat, W. (1995). *Rev. Sci. Instrum.* **66**, 1–14.